

Fluid-dynamic properties and wetting behavior of coating inks for roll-to-roll production of polymer-based solar cells

L. Wengeler, K. Peters, M. Schmitt, T. Wenz,
P. Scharfer, W. Schabel

© American Coatings Association & Oil and Colour Chemists' Association 2013

Abstract In the last decade, semiconducting and conducting materials were developed that can be processed by solvent-based deposition to form functional layers or complete electronic devices. These materials are typically synthesized in laboratory scale quantities and tested on small spin-coated substrates, whereas the final goal is to produce them on flexible substrates in a continuous roll-to-roll process. To enable a fast scale up and optimization, fluid-dynamic properties have to be known. Here, we present viscosity and surface tension data for typical material systems, applied in polymer-based solar cells. Materials presented include water-based polymer dispersions (hole-conducting and high-conductive PEDOT:PSS types), solvent-based anorganic nanoparticle dispersions (silver nanoparticle ink, hole-blocking ZnO nanoparticle ink), and dissolved organic molecules and polymers (P3HT:PCBM photoactive blend). Predictive models are proposed to approximate viscosity and surface tension for these materials at various compositions. As well, corona treatment is used to modify the surface energy of P3HT:PCBM and described as a function of web speed and corona power. The importance of material properties is demonstrated by predicting stable conditions for a slot-die coating process. A simple drying simulation

highlights the possibility of using property models to investigate wetting problems.

Keywords Polymer solar cell, Organic photovoltaic, Printed electronics, Surface tension, Viscosity, Surface energy, Wetting, Coating, Slot die, PEDOT:PSS, P3HT, PCBM, ZnO nanoparticles, Ag nanoparticles, Corona, Surfactant, Triton, Surfactant

Introduction

Polymer-based solar cells (PSCs) can be manufactured in a continuous roll-to-roll process as a low cost regenerative energy source.¹ Coating ink properties and film thicknesses of 30 to 200 nm are challenging with respect to the manufacturing process, which itself has an important impact on film properties and cell efficiencies.² Whereas record power conversion efficiencies of PSCs have crossed the value of 10%,³ the average efficiencies of large area cells are much lower. Though a number of groups have successfully proven the principle of roll-to-roll manufacturing of PSC (e.g., references 4–10) with a record efficiency of 3.5%,⁸ developing a stable process for large area coating and drying, with high average efficiencies and reliability, is still one of the major challenges for this technology. To allow for a controlled scale up and a fast optimization, material properties—such as viscosity and surface tension—have to be known (Fig. 1).

In this article we present viscosity data of typical ink compositions and introduce predictive models for commercial materials (“[Viscosity](#)”). Surface tension of inks and surface energy of substrates will be discussed in the section on “[Surface tension](#)” and “[Surface energy](#),” respectively. Finally, the importance of material properties for coating (“[Coating stability](#)”) and wetting stability (“[Wetting stability](#)”) will be highlighted.

This paper was presented at the 16th International Coating Science and Technology Symposium, September 9–12, 2012, in Atlanta, GA (USA).

L. Wengeler (✉), K. Peters, M. Schmitt,
T. Wenz, P. Scharfer, W. Schabel
Institute of Thermal Process Engineering, Thin Film
Technology (TFT), Karlsruhe Institute of Technology
(KIT), Karlsruhe, Germany
e-mail: Lukas.Wengeler@kit.edu



Fig. 1: Polymer-based solar cell, coated on a flexible PET substrate

Experimental

Materials

The materials investigated in this article, and their function within the PSC, are illustrated schematically in Fig. 2.

The photoactive layer—a bulk hetero-junction of polymer (here poly-3-hexylthiophene-2,5-diyl (P3HT), P200, BASF) and fullerene (here phenyl-C61-butyric acid methyl ester (PCBM) PC₆₀BM, Solenne BV)—is sandwiched between an electron-blocking layer (here poly-3,4-ethylenedioxythiophene:poly-styrenesulfonate (PEDOT:PSS), VPAI40.83, Heraeus) and a hole-blocking layer (here zinc oxide (ZnO) ZnO, ZN2225 Nanoarc, Alfa Aesar). The transparent electrode can be either a sputtered indium–tin oxide (ITO) layer or a coated high-conductive PEDOT:PSS type (here PH1000 or PH500, Heraeus). The reflective electrode can be either a coated silver nanoparticle layer (here PR020, InkTec) or an evaporated metal film.

As prices of these materials are quite high (e.g., 150 €/g PCBM¹¹) model systems were used for fundamental coating experiments. Polystyrene (PS, Art.N.: 9151.1, Carl-Roth) colored with Sudan3 (1/30th of PS solid content, Art.N.: 4711.1, Carl-Roth) and polyacrylamide (PAA, Art.N.:3048.1, Carl-Roth) colored with Amidoschwarz (Art.N.: 9590.1, Carl-Roth) were used as model systems for organic solvent or water-based inks, respectively.

The photoactive material was dissolved in chlorinated solvents (here chlorobenzene (CB), dichlorobenzene (DCB), and chloroform (CF)), while xylene (XYL) was used as an alternative nonchlorinated solvent. The hole-blocking ZnO nanoparticles were received as a dispersion stabilized by a ligand (propyl-

ene glycol monomethyl acetate (PGMEA)) and diluted with a nonpolar organic solvent (here acetone). PEDOT:PSS, applied either as electron-blocking layer or as transparent electrode, was received as water-based dispersion. Small amounts of additive were added to improve conductivity (dimethyl sulfoxide, DMSO) and wetting behavior (methanol (MeOH), isopropanol (IPA), or Triton X-100 (TX-100)). Silver nanoparticles were received as an IPA-based dispersion and diluted further with IPA to adjust material properties and solid content.

Methods

Viscosity measurements were carried out with a cone plate rotational rheometer (MCR101, Anton Paar GmbH). Surface tension was determined by the pendant drop method and surface energy calculated from sessile drop measurements with a contact angle measurement system (EasyDrop, Krüss).

To insure reproducible results, all dispersions (e.g., PEDOT:PSS, PR-020) were submerged in an ultrasonic bath (S40-M, Elmasonic) for 10 min before the experiments. The equipment and procedure for coating experiments is described elsewhere.^{12,13} Due to small coating gaps of less than 50 μm, the slot-die coater was mounted on a runner system to adjust the relative distance between lip and substrate. Instead of a backing roll, the substrate was led over a high precision granite plate to minimize disturbances due to the tolerance of bearing and roll.

Electrode films were annealed for 30 min at 120°C in nitrogen atmosphere, before characterization with a four-point probe, conductivity measurement system. Corona treatment was conducted with an in-line unit (1.5 kW, Pillar) and an electrode distance of 1.09 mm.

Material properties

Many organic materials have been developed in the last decade to enhance efficiency and lifetime of PSCs (see e.g., reference 14). These materials are typically produced on a laboratory scale and available in small quantities only. An empirical approach for finding optimized process conditions for a production scale process requires a large amount of coating material and is therefore often not feasible.

We will thus present data for material properties that are relevant for the coating process and propose methods to predict them. Table 1 shows composition, density, viscosity, and surface tension for an exemplary system for each of the layers displayed in Fig. 1.

Due to the typically small solid content (for all systems except PR-020 and ZnO; see Table 1), the density ρ of the ink can be approximated for an ideal mixture of i solvents without a measured value for the density of the dissolved or dispersed solid:

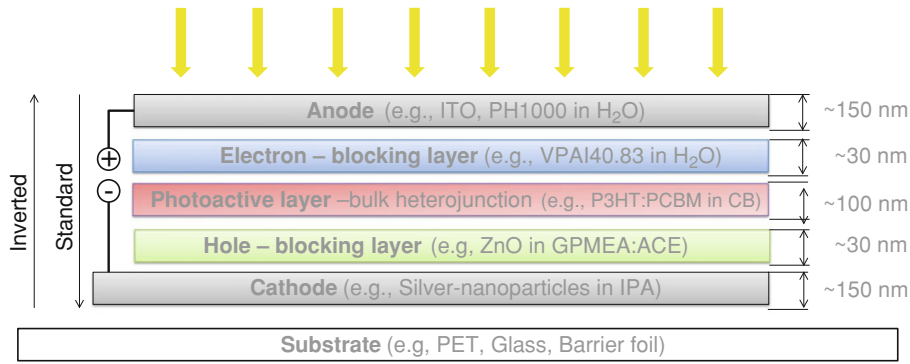


Fig. 2: Schematic sketch of a polymer-based solar cell showing typical material systems and their function within the cell architecture

Table 1: Overview of fluid-dynamic properties of material systems typically applied in polymer-based solar cells

System	Solid m:m	Density (g/cm ³)	Solvent	Density (g/cm ³)	Viscosity (mPa.s)		Surface tension (mN/m)	x _{Solid} (wt%)
					5 1/s	1000 1/s		
Printed electrodes	PR-020	~10.49	IPA	0.79	11	8	21.6	17
Active layer	PCBM:P3HT 0.8:1	~1.3	DCB	1.3	4.4	4.3	33	3.1
Transparent cond. layer	PH500	1.62	H ₂ O	1	60.3	12.5	69.2	1.27
Electron-blocking layer	VPAI 4083	1.62	H ₂ O	1	4	3.9	~69.2	1.36
Hole-blocking layer	ZnO	5.61	GPMEA	0.97	5	4.4	19.2	40.3
Model AL	PS	1.05	XYL	0.86	3.6	3.9	23.1	3
Model HCL	PAA	0.8	H ₂ O	1	70.2	24.5	71.8	0.34

$$\frac{1}{\rho} = \frac{x_{\text{Solid}}}{\rho_{\text{Solid}}} + \sum_i \frac{x_i}{\rho_i} \approx \sum_i \frac{x_i}{\rho_i} \quad \text{for } x_{\text{Solid}} \ll 1, \quad (1)$$

where x is the mass fraction and the lower index represents the component.

In contrast, viscosity depends on material and composition and may be temperature and shear-rate dependent.

Viscosity

Shear-rate dependent viscosity of PEDOT:PSS

Viscosity may be described as a function of solid mass fraction x_{Solid} (in wt%) by an empirical fit to a second-order polynomial

$$\eta_{0,20^\circ\text{C}}(x_{\text{Solid}}) = c_1 \cdot x_{\text{Solid}}^2 + c_2 \cdot x_{\text{Solid}} + \eta_{\infty}, \quad (2)$$

shear rate $\dot{\gamma}$ (in 1/s) by a Carreau-Yasuda model (see e.g., reference 15)

$$\eta_{20^\circ\text{C}}(x_{\text{Solid}}, \dot{\gamma}) = \eta_{\infty} + (\eta_{0,20^\circ\text{C}} - \eta_{\infty}) \left[1 + (\lambda \cdot \dot{\gamma})^2 \right]^{\frac{n-1}{2}}, \quad (3)$$

and temperature T (in K) by an Arrhenius relationship (see e.g., reference 15)

$$\eta(x_{\text{Solid}}, \dot{\gamma}, T) = \eta_{20^\circ\text{C}}(x_{\text{Solid}}, \dot{\gamma}) \cdot e^{\frac{E_A}{R} \left(\frac{1}{T} - \frac{1}{293.14 \text{ K}} \right)}. \quad (4)$$

The solid mass fraction of undiluted PEDOT:PSS dispersions was determined to be 1.97, 1.27, or 1.36 wt% for undiluted PH1000, PH500, and VPAI4083, respectively. Model parameters for three commercial PEDOT:PSS dispersions are summarized in Table 2.

Newtonian viscosity of solvent-based inks

The photoactive materials, dissolved in organic solvents, exhibit Newtonian behavior at low solid concentrations and can be described at 20°C by

$$\eta_{20^\circ\text{C}}(x_{\text{Ful}}, x_{\text{Pol}}) = k_3 \cdot x_{\text{Pol}}^2 + k_2 \cdot x_{\text{Pol}} + k_1 \cdot x_{\text{Ful}} + \eta_{\infty} \quad (5)$$

Table 2: Parameter values for concentration, shear rate, and temperature-dependent viscosity models

PEDOT:PSS type	c_1 (mPa.s/wt% ²)	c_2 (mPa.s/wt%)	λ (s)	n (-)	E_A/R (K)
PH1000	4.064	6.351	0.0185	0.718	1205
PH500	22.24	8.308	0.054	0.688	1513
VPAI4083	-0.4166	2652	-	-	1906

Parameters were fitted to data in the following range: $x_S < 0.0197$; $10 < \dot{\gamma} < 10,000$; and $10^\circ\text{C} < T < 50^\circ\text{C}$

Table 3: Parameter values (equation 5) for concentration dependent viscosity of solvent-based inks for OPV at 20°C

Material	k_3 (1/wt% ²)	k_2 (1/wt%)	k_1 (1/wt%)	$x_{S,Max}$ (wt%)
P3HT, P200, BASF	0.8287	-0.0629		2
PC ₆₀ BM, Solenne BV			0.454	4
ZnO, Alfa Asear	0.0029	-0.0175		40
PR-020	0.0218	0.0555		20
Polystyrene	0.1723	0.4196		8

Viscosity was fitted for a solid mass fraction $0 < x < x_{S,Max}$ and may be considered as shear-rate independent in this concentration range

where x_{Pol} and x_{Full} are the solid mass fraction (in wt%) of polymer and fullerene, respectively. The model parameters for an exemplary material system of P3HT (P200, BASF) and PCBM are given in Table 3. Note that for each new polymer (including polymers of similar structure but different molecular weight) the parameters k_3 and k_2 and for new fullerene derivatives the parameter k_1 have to be measured.

Once the parameters are determined, it is possible to estimate the viscosity at various compositions (polymer fullerene ratio, solid mass fraction, and solvent composition) without further measurements as demonstrated in Fig. 3.

Based on viscosity data of P3HT in CB (blue diamonds) and PCBM in DCB (red squares), the model parameters were fitted (solid blue and red line). With these parameters and equation (5) the viscosity of a blend, with mass ratio 1:0.8 of P3HT:PCBM in CB, can be estimated. The model (broken green line) is in good agreement with the measured data (green triangles) and their second-order polynomial fit (solid green line).

Table 3 also gives parameters for ZnO (Zn2225) and silver nanoparticle (PR-020) dispersions and PS as a model system.

Solvent viscosity

The infinite shear viscosity η_∞ in equation (3) is equal to the solvent viscosity (equations 2 and 5) and can—depending on the composition—significantly affect the overall viscosity value (Fig. 4). Temperature-dependent viscosity of pure solvents can be found in material property literature (e.g., reference 16) and

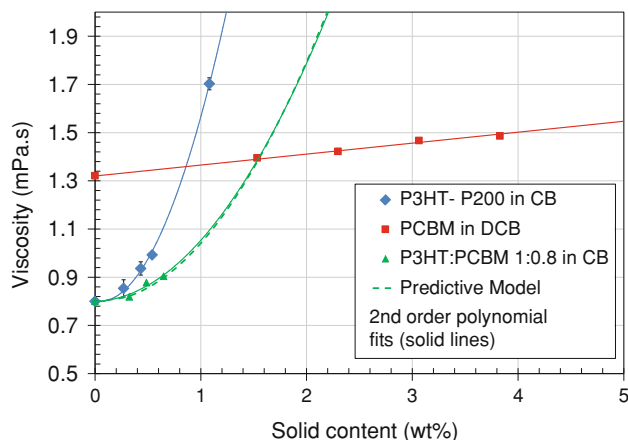


Fig. 3: Viscosity of photoactive materials, P3HT (blue), PCBM (red), and P3HT:PCBM (green, dissolved in CB or DCB). The additive model for the blend (broken green line) is in good agreement with measured data (Color figure online)

data for relevant binary solvent–water mixtures (the data for methanol and ethanol was taken from Gonzalez et al.¹⁷ and own measurements) are shown in Fig. 4. DMSO and EG are often used as conductivity enhancing additives in PEDOT:PSS dispersions (see e.g., reference 18), alcohols are often added to improve wetting behavior (see e.g., reference 19).

Whereas the addition of small amounts (<5 wt%) of high viscous additives, ethylene glycol, DMSO, and Triton X (TX-100 not shown here) has little impact on overall viscosity, the addition of 20 wt% ethanol can increase the solvent viscosity by a factor of 2.7 (1.7 mPa.s absolute). The viscosity of pure solvents (in mN/m) can be computed as a function of temperature (in K) using the correlation and data compiled by Yaws.¹⁶ Teja and Rice²⁰ employ a generalized corresponding states method to predict viscosity of liquid mixtures (solid lines in Fig. 4) based on a binary interaction coefficient Ψ_{ij} (see Table 4). Whereas most solvent mixtures can be predicted with reasonable accuracy, highly nonideal mixtures (such as EG:H₂O) may have to be fitted to higher order polynomial equations.

Surface tension

The surface tension of inks for OPV is dominated by the solvent composition. For typical solid concentra-

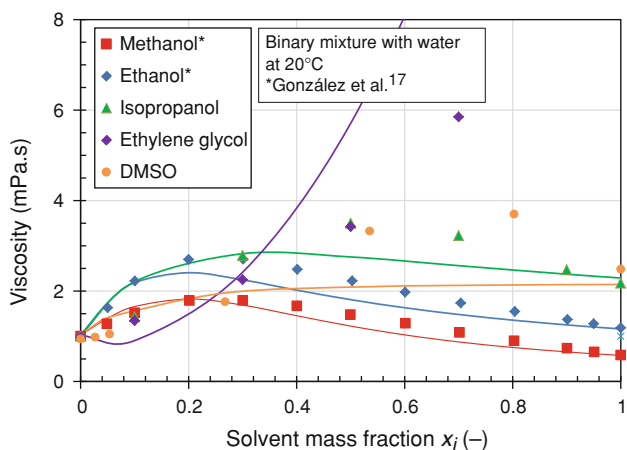


Fig. 4: Experimental data for the viscosity of binary solvent–water mixtures. The data for methanol and ethanol was taken from Gonzalez et al.,¹⁷ solid lines represent binary fits based on the model of Teja and Rice²⁰

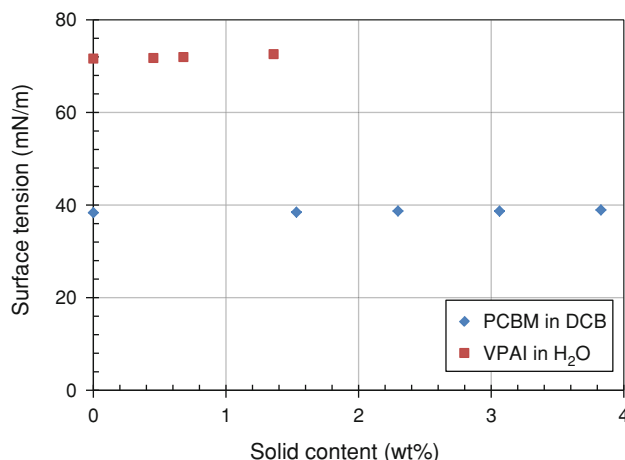


Fig. 5: Surface tension of PCBM and PEDOT:PSS do not depend on solid mass fraction

Table 4: Interaction parameters for the calculation of viscosity and surface tension of binary solvent–water mixtures

	Viscosity $\Psi_{i,j}$	Surface tension		
		σ_2 (mN/m)	e_1	e_2
Methanol	1.34 ¹	23.5	0.899 ²	0.777 ²
Ethanol	1.36 ¹	23.4	0.963 ²	0.897 ²
Isopropanol	1.27 ³	22.4	0.984 ²	0.970 ²
Dimethyl sulfoxide	1.08 ³	43.8	0.869 ³	0.603 ³
Ethylene glycol	0.82 ³	45.9	0.826 ³	0.867 ³

¹ Teja and Rice,²⁰ ² Connors and Wright,²² ³ this work

tions there is no significant impact on surface tension (see Fig. 5).

The temperature dependence of pure solvents is tabulated and fitted to a linear equation by Jasper²¹ and a model for the surface tension of binary mixtures with water is given by Conors and Wright²²:

$$\sigma = \sigma_{\text{H}_2\text{O}} - \left[1 + \frac{e_1 \tilde{x}_{\text{H}_2\text{O}}}{1 - e_2 \tilde{x}_{\text{H}_2\text{O}}} \right] \tilde{x}_{\text{Solvent}} (\sigma_{\text{H}_2\text{O}} - \sigma_{\text{solvent}}). \tag{6}$$

Here \tilde{x}_i and σ_i are the molar fractions and surface tension of component i , and e_1 and e_2 are binary interaction parameters (see Table 4). Figure 6 shows the surface tension of water solvent mixtures as a function of the solvent mass fraction. The surface tension shows a progressive increase towards a solvent content of zero for all mixtures.

In contrast to the low surface tensions (SFT) of alcohols (<25 mN/m), the SFT of DMSO and ethylene glycol (EG) mixtures remain above 40 mN/m. To enable wetting on low surface energy (SFE) substrates, such as an untreated P3HT:PCBM photoactive layer ($\text{SFE}_{\text{P3HT:PCBM, Untreated}} = 29.7 \text{ mN/m}$), the SFT of these dispersions has to be

decreased by adding a surfactant. Figure 7a shows the SFT of an aqueous dispersion with 90 vol.% PH1000 and 5 vol.% DMSO as a function of the mass fraction of the nonionic surfactant Triton X-100 (blue diamonds). Compared to TX-100 mixtures with pure water (red squares), the critical micelle concentration is shifted to a higher TX-100 mass fraction of 0.1 wt% (= 0.17 mol/l).

Up to a solid mass fraction of 0.5 wt% TX-100, the specific conductivity of coated films does not decrease with surfactant concentration (Fig. 7b). However, higher concentrations lead to a decrease in specific conductivity and should be avoided in a technical process.

Surface energy

Even though, based on the data presented above, a TX-100 concentration of 0.1 wt% should be sufficient to lower the surface tension to its final value, de-wetting may still occur in a technical coating process.

The coating of a thin film (here typically below 20 μm wet thickness) creates a large surface area and the dynamic surface tension, immediately after crea-

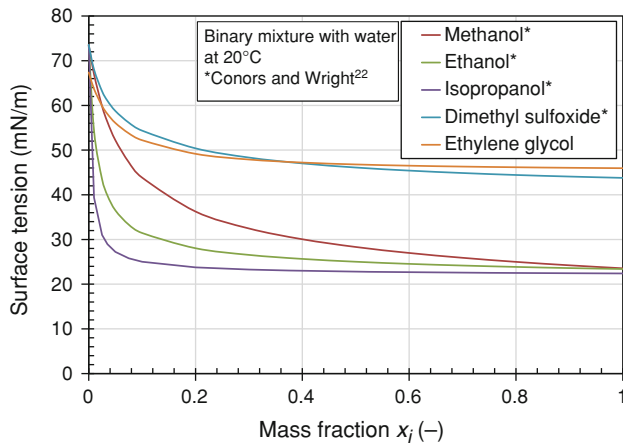


Fig. 6: Surface tension of binary solvent:water mixtures. Asterisk represents the data are taken from reference (22) and own measurements

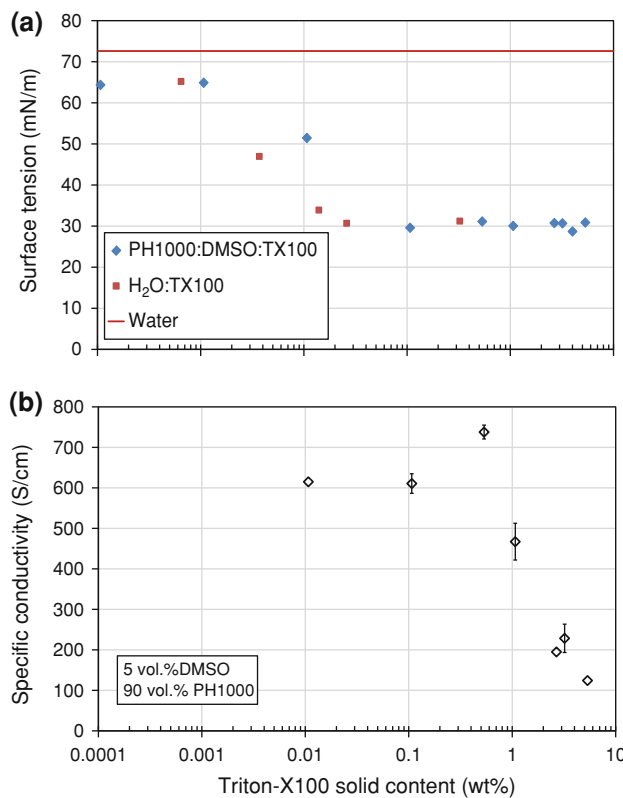


Fig. 7: Surface tension (blue diamonds; (a)) and specific conductivity of the coated film (b) for a dispersion of high conductive polymer (90 vol.% PH1000, 5 vol.% DMSO) as a function of TX-100 solid mass fraction. The surface tension of a water TX-100 mixture is shown as reference (red squares; (a)) (Color figure online)

tion of the surface, may be higher than its equilibrium value. Voigt et al.¹⁹ showed that a treatment of the photoactive layer with oxygen plasma may improve wetting without sacrificing device efficiency. In contin-

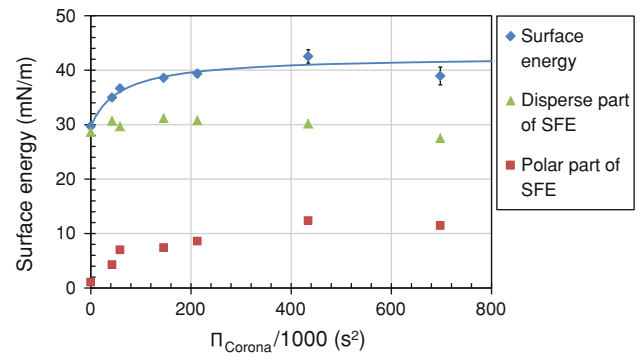


Fig. 8: Surface energy of a plasma-treated P3HT:PCBM film as a function of treatment intensity (blue diamonds). The solid line is a fit to equation (10). Disperse-part and polar-part of the SFE are shown by triangles and squares, respectively (Color figure online)

uous coating lines an air-plasma treatment (corona treatment) is often used to modify surface energy. Here, the residence time is a function of the coating speed so that the power of the corona generator has to be adjusted to achieve a desired surface activation. Wolf and Sparavigna²³ expressed the intensity of a corona treatment as product of power times residence time divided by area. In this article, we chose instead to define the treatment intensity by:

$$\Pi_{\text{Corona}} = \frac{P \cdot \tau^3}{A_{\text{Corona}} \cdot \text{SFT}_{\text{Min}}}, \quad (7)$$

with P being the power of the corona generator, τ the residence time, A_{Corona} the area on which the corona is applied, and SFT_{Min} the minimal surface tension (here equivalent to the untreated value). The residence time is a function of web speed (u) for a given length in web direction (L) and width perpendicular to the web direction (W) of the corona gap. Equation (7) becomes:

$$\Pi_{\text{Corona}} = \frac{P \cdot L^2}{u^3 \cdot W \cdot \text{SFT}_{\text{Min}}}, \quad (8)$$

with $\tau = \frac{L}{u}$ and $A_{\text{Corona}} = L \cdot W$.

Figure 8 shows the surface energy and its disperse and polar part of corona treated P3HT:PCBM blends as a function of treatment intensity. The overall surface energy can be increased up to a value of 42.5 mN/m and the steepest increase occurs at low treatment intensities ($\Pi_{\text{Corona}} < 200,000 \text{ s}^2$; Figure 8).

The SFE can be expressed in a dimensionless form as:

$$\Pi_{\text{SFE}} = \frac{\text{SFT} - \text{SFT}_{\text{Min}}}{\text{SFT}_{\text{Max}} - \text{SFT}_{\text{Min}}}. \quad (9)$$

Corona treatment of PET (Melinex OD) substrates with variable coating speed (triangles) and variable

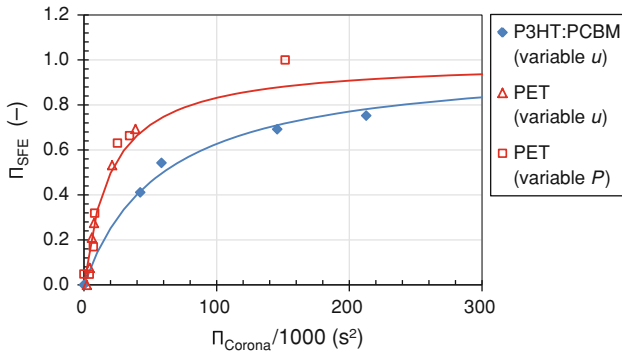


Fig. 9: Dimensionless surface energy (defined in equation 9) as a function of treatment intensity (defined by equation 7). Diamonds represent the surface energy of a photoactive blend (P3HT:PCBM) whereas triangles and squares represent as PET substrate treated with variable velocity and power, respectively. The solid lines represent least sum of square fits of equation (10)

power settings (squares) can be expressed by the same correlation (blue line in Figs. 8 and 9) when using equation (7) as definition of the corona treatment intensity:

$$\Pi_{SFE} = \frac{\Pi_{Corona}}{\frac{1}{f} + \Pi_{Corona}}, \quad (10)$$

where f is the initial slope of the correlation depending on the set-up (e.g., efficiency of corona generator) and treated substrate (e.g., thickness and material of the substrate). Using this correlation it is thus possible to select the required corona power for a given coating speed in order to achieve a desired increase in SFE.

The correlation is valid for low power intensities (<200,000 1/s²) and in-line corona treatment systems where the coating takes place mere minutes after the corona treatment. For plasma ovens which are often used to treat glass substrates in laboratories, the surface tension decreases linearly over time after the treatment. The half-life time of the plasma treatment lies in the order of minutes to days, depending on the type of substrate and humidity during processing (e.g., ITO ~ 90 min @ ~75% rH).

Process stability

Coating stability

For a slot-die coating process the limiting operating variables are coating speed u and wet film thickness D . The coating speed can be expressed in a dimensionless form as capillary number Ca :

$$Ca = \frac{\eta u}{\sigma}, \quad (11)$$

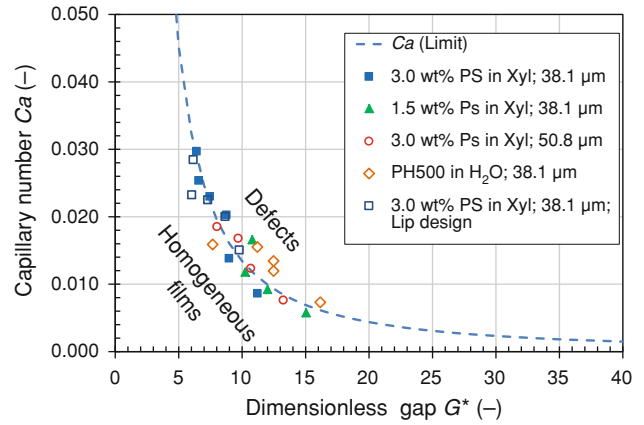


Fig. 10: Dimensionless coating window for slot-die coating of aqueous and solvent-based inks for PSCs. The dashed line represents the experimentally determined limiting coating speed for a given wet film thickness for slot-die coating of OPV materials without vacuum chamber

where η is the viscosity and σ the surface tension. The inverse film thickness can be expressed in a dimensionless form as dimensionless gap width:

$$G^* = \frac{G}{D}, \quad (12)$$

where G is the distance between die-lip and substrate. The shear-rate in the coating gap, needed to determine the viscosity for nonNewtonian inks (e.g., PH1000), can be approximated for a Couette flow by:

$$\dot{\gamma} = \frac{u}{G}. \quad (13)$$

The coating limit for semiconducting inks, determined by an equilibrium of capillary and viscous forces at the meniscus below the die-lip, was presented in reference (12) for organic solvents. Figure 10 shows additional data points for an aqueous PEDOT:PSS dispersion (diamonds) and a slot-die with a different lip design (open squares).

The new data is consistent with previous results for PS in XYL demonstrating that the limiting capillary number:

$$Ca_{Limit} = n \cdot \left(\frac{2}{G^* - 1} \right)^{3/2} \quad \text{with } n = 0.128, \quad (14)$$

is valid for various compositions, coating tools, and coating parameters.

Wetting stability

Coating of aqueous dispersions may be challenging due to the high surface tension of water. Figure 11 shows

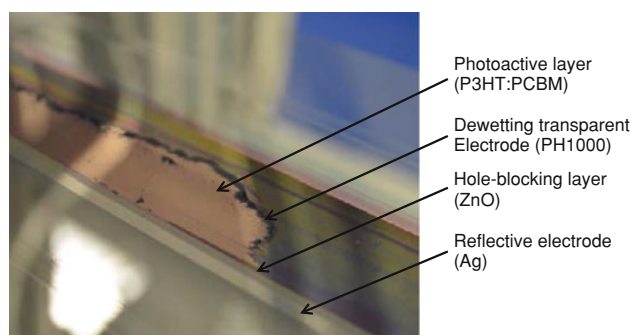


Fig. 11: De-wetting of a high conductive polymer film on a multilayer OPV stack

an example for complete de-wetting of a PH1000 dispersion on a photoactive layer.

As discussed above, the surface tension of the ink can be decreased by the addition of alcohol or surfactant, and the surface energy of the photoactive layer may be increased by in-line corona treatment. A too high surfactant concentration or a too intense corona treatment, however, may have negative effects on the functionality of the film and the efficiency of the device.

Though initial wetting is mandatory to form functional layers for OPV, many wetting-related defects occur during the drying process. As the film dries, composition and temperature change and a film that was initially homogeneous may become unstable. Using the models presented above, it is now possible to compute the driving force (surface tension) and the retarding force (viscosity) for de-wetting in a numerical simulation of the drying process.

Figure 12 shows a drying simulation of a PEDOT:PSS dispersion (PEDOT:PSS + 15 wt% IPA) at low (A: 40% rH) and high (B: 85% rH) relative humidity. The calculations were simplified, assuming ideal solvent behavior, an adiabatic film without heat capacity and no diffusional mass transport limitation within the film. The convective and radiative heat transfer coefficients were set to $50 \text{ W}/(\text{m}^2 \text{ K})$ and $5 \text{ W}/(\text{m}^2 \text{ K})$, respectively. Film thickness (blue line), surface tension (red line), and zero shear viscosity (green line) are plotted as a function of drying time. A significant amount of IPA remains within the film until viscosity and SFT increase in the last seconds of the drying process at low relative humidity. At a high relative humidity the mass transport of water is slower and the surface tension approaches the value of pure water, whereas viscosity remains less than $10 \text{ mPa}\cdot\text{s}$ after 30 s.

Even though the simplifications above do not allow for quantitative evaluation, critical wetting conditions can be determined. A high surface energy and low viscosity for a critical time span indicate an undesirable operating point.

Similar simulations showed that the addition of the low boiling point solvent DMSO slows down the drying, so that the addition of surfactant is necessary

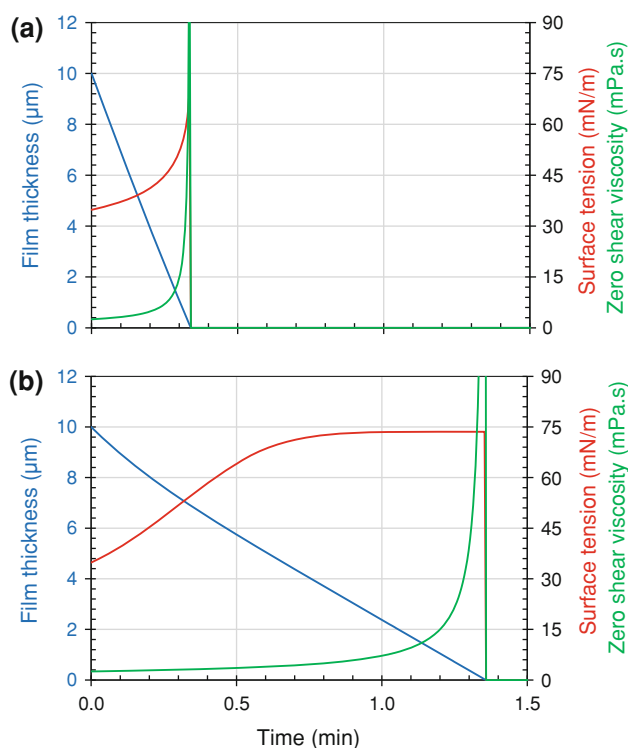


Fig. 12: Simplified drying simulation of a PEDOT:PSS (0.15 wt% IPA) dispersion at a relative humidity of 40% rH (a) and 85% rH (b). At high humidity, a high surface tension and low viscosity is present over a period of almost 1 min, favoring a de-wetting

even at low relative humidity. Evaporative cooling of a P3HT:PCBM film may cause condensation of a water film onto the organic film and may be the reason for wetting related defects, observed for slow drying photoactive layers.

Summary and outlook

Conductive (transparent or reflective) and semiconductive (hole-blocking, electron-blocking, or photoactive) layers can be prepared by solvent-based deposition using organic and hybrid material systems. Viscosity and surface tension data for typical material systems, needed to produce a PSC, are presented. Quantitative models to estimate these properties as a function of compositions, shear-rate, and temperature were proposed or reviewed. As well, the surface energy of a photoactive P3HT:PCBM layer was measured as a function of corona treatment intensity and fitted to a model that describes the surface energy as a function of web speed and corona generator power. Optimization of composition and corona treatment to achieve highest functionality can be facilitated using the methods presented here and is the subject of current research.

A dimensionless coating window for a slot-die coating process illustrates the importance of material

properties. For an organic electronic ink with given viscosity and surface tension, the minimal stable thickness at a given speed can be predicted. Even for stable coating conditions, the wet films may still de-wet during the drying process. A simple drying simulation shows the potential of the property models presented before for the investigation of wetting issues. A more rigorous simulation of the drying process in combination with the property models presented here might explain and subsequently circumvent wetting- or drying-related problems for the roll-to-roll production of functional films in PSCs.

Acknowledgments We gratefully acknowledge the financial support of the Baden-Württemberg-Stiftung.

References

1. Brabec, CJ, *Organic Photovoltaics Materials, Device Physics, and Manufacturing Technologies*. Wiley-VCH, Weinheim, 2008
2. Peet, J, et al., “The Role of Processing in the Fabrication and Optimization of Plastic Solar Cells.” *Adv. Mater.*, **21** (14–15) 1521–1527 (2009)
3. National Renewable Energy Laboratory, *Research Cell Efficiency Records* (2012)
4. Krebs, FC, et al., “A Complete Process for Production of Flexible Large Area Polymer Solar Cells Entirely Using Screen Printing—First Public Demonstration.” *Sol. Energy Mater. Sol. Cells*, **93** (4) 422–441 (2009)
5. Kopola, P, et al., “High Efficient Plastic Solar Cells Fabricated with a High-Throughput Gravure Printing Method.” *Sol. Energy Mater. Sol. Cells*, **94** 1673–1680 (2010)
6. Blankenburg, L, et al., “Reel-to-Reel Wet Coating as an Efficient Up-Scaling Technique for the Production of Bulk-Heterojunction Polymer Solar Cells.” *Sol. Energy Mater. Sol. Cells*, **93** (4) 476–483 (2009)
7. Galagan, Y, et al., “Technology Development for Roll-to-Roll Production of Organic Photovoltaics.” *Chem. Eng. Process.*, **50** (5–6) 454–461 (2011)
8. Park, HJ, et al., “A Facile Route to Polymer Solar Cells with Optimum Morphology Readily Applicable to a Roll-to-Roll Process Without Sacrificing High Device Performances.” *Adv. Mater.*, **22** E247–E253 (2010)
9. Zimmermann, B, et al., “ITO-Free Flexible Inverted Organic Solar Cell Modules with High Fill Factor Prepared by Slot Die Coating.” *Sol. Energy Mater. Sol. Cells*, **95** (7) 1587–1589 (2011)
10. Steim, R, et al., “Organic Photovoltaics for Low Light Applications.” *Sol. Energy Mater. Sol. Cells*, **95** (12) 3256–3261 (2011)
11. Solenne BV, <http://www.solennebv.com/price%20lists.htm>, 2012
12. Wengeler, L, et al., “Comparison of Large Scale Coating Techniques for Organic and Hybrid Films in Polymer Based Solar Cells.” *Chem. Eng. Process.* (2012). doi:10.1016/j.cep.2012.03.004
13. Wengeler, L, et al., “Investigations on Knife and Slot Die Coating and Processing of Polymer Nanoparticle Films for Hybrid Polymer Solar Cells.” *Chem. Eng. Process.*, **50** (5–6) 478–482 (2011)
14. Helgesen, M, Sondergaard, R, Krebs, FC, “Advanced Materials and Processes for Polymer Solar Cell Devices.” *J. Mater. Chem.*, **20** (1) 36–60 (2010)
15. Macosko, C, Larson, R, *Rheology: Principles, Measurements, and Applications*. Wiley-VCH, New York, 1994
16. Yaws, C, *Chemical Properties Handbook: Physical Thermodynamic, Environmental, Transport, Safety and Health Related Properties for Organic and Inorganic Chemicals*. McGraw-Hill, New York, 1999
17. Gonzalez, B, et al., “Density, Dynamic Viscosity, and Derived Properties of Binary Mixtures of Methanol or Ethanol with Water, Ethyl Acetate, and Methyl Acetate at T = (293.15, 298.15, and 303.15) K.” *J. Chem. Thermodyn.*, **39** (12) 1578–1588 (2007)
18. Dimitriev, OP, et al., “PEDOT:PSS Films—Effect of Organic Solvent Additives and Annealing on the Film Conductivity.” *Synth. Met.*, **159** (21–22) 2237–2239 (2009)
19. Voigt, MM, et al., “Gravure Printing Inverted Organic Solar Cells: The Influence of Ink Properties on Film Quality and Device Performance.” *Sol. Energy Mater. Sol. Cells*, **105** 77–85 (2012)
20. Teja, AS, Rice, P, “Generalized Corresponding States Method for the Viscosities of Liquid-Mixtures.” *Ind. Eng. Chem. Fundam.*, **20** (1) 77–81 (1981)
21. Jasper, JJ, “The Surface Tension of Pure Liquid Compounds.” *J. Phys. Chem. Ref. Data*, **1** (4) 841–1010 (1972)
22. Connors, KA, Wright, JL, “Dependence of Surface Tension on Composition of Binary Aqueous-Organic Solutions.” *Anal. Chem.*, **61** (3) 194–198 (1989)
23. Wolf, R, Sparavigna, AC, “Role of Plasma Surface Treatments on Wetting and Adhesion.” *Engineering*, **2** (6) 397–402 (2010)